

Design of High-Speed Direct-Connected Permanent-Magnet Motors and Generators for the Petrochemical Industry

Cassandra Bailey, *Member, IEEE*, Daniel M. Saban, *Senior Member, IEEE*, and Paulo Guedes-Pinto, *Member, IEEE*

Abstract—This paper reexamines some of the usual assumptions in deploying synchronous machines in multi-megawatt high-speed applications. A viable design that can operate at common gas turbine speeds and power ratings is presented with a focus on rotor capability and cooling system performance. The models used in the analysis are validated using test data from a similar topology machine with a higher operating speed but lower power as well as a prototype machine built based on the design presented.

Index Terms—Generator, high speed, motor, permanent magnet (PM), synchronous.

I. INTRODUCTION

HIGH-SPEED machines have become an increasingly attractive design solution in applications where it is desirable to eliminate gearboxes and their associated accessory systems. For example, high-speed electric motors with variable-speed drives have been shown to have an advantage over gas turbines as a prime mover for natural-gas compressor applications when both environmental and economic factors are considered [1], [2]. Another advantageous application for high-speed machines is power generation when directly coupled to a gas turbine. High-speed machines can be operated at frequencies an order of magnitude above line frequency, which allows the machines to be smaller than conventional machines in the same power rating which yields significantly higher power density than with a conventional alternative.

Due to the better power-to-weight ratio, smaller size, and higher efficiency compared to induction machines, high-speed permanent-magnet (PM) machines are a topology being recently considered for subsea, offshore, and shipboard applications [3], [4]. Both synchronous (PM or wound-field) and asynchronous (induction) machines have been considered for these applications; however, there are significant advantages inherent in a PM machine. Therefore, the differences between these machines warrant further discussion.

Paper PID-08-08, presented at the 2007 IEEE Petroleum and Chemical Industry Technical Conference, Calgary, AB, Canada, September 17–19, and approved for publication in the IEEE TRANSACTIONS ON INDUSTRY APPLICATIONS by the Petroleum and Chemical Industry Committee of the IEEE Industry Applications Society. Manuscript submitted for review December 1, 2007 and released for publication November 19, 2008. Current version published May 20, 2009.

The authors are with Direct Drive Systems, Cerritos, CA 90703 USA (e-mail: cbailey@directdrivesystems.net; saban@ieee.org; pguedes-pinto@directdrivesystems.net).

Color versions of one or more of the figures in this paper are available online at <http://ieeexplore.ieee.org>.

Digital Object Identifier 10.1109/TIA.2009.2018964

The wound-field synchronous machines discussed by LaGrone *et al.* [2] and Gilon [5] and the squirrel-cage induction machines discussed by Arkkio *et al.* [6] and Evon and Schiferl [7] were discounted for high-speed multimegawatt applications because of the complex rotor construction typical to these types of machines. PM synchronous machines and solid rotor induction machines do not suffer from many of the same difficulties [8], as they do not have a field winding or a rotating rectifier and can consequently achieve a higher rotor stiffness with the same rotor OD and magnetic length. The difference between high-speed multimegawatt PM machines and their lower powered brethren as studied by Melfi *et al.* [9] and Bianchi *et al.* [10] should also be highlighted.

High-speed PM machines typically have surface-mounted magnets and are sleeved. Many low-power designs can be achieved without a sleeve or with a sleeve of insignificant thickness. A high-speed multimegawatt PM machine will typically require a sleeve several times larger than the mechanical gap or the order of magnitude of the magnet thickness. Laminated rotor cores and/or embedded magnets considered in some low-power designs do not offer either the radial stiffness or mass containment required for many applications. The sleeve provides the containment, and a solid rotor core or hub provides stiffness. Common sleeve materials are nonmagnetic high-strength alloys [3], premolded graphite or carbon composites, and wound-in-place carbon fiber or carbon-fiber composites. Of these, the carbon-fiber winding offers the highest strength while providing minimal conduction paths for eddy currents induced by air-gap flux disturbances.

While Arkkio *et al.* [6] were primarily focused on high-speed applications of not more than 1 or 2 MW, the observation that induction machines will require a larger diameter than an equivalent PM machine should not be lost on the reader. As the power rating becomes higher, the rotor speeds become lower, but the diameters grow. Arkkio *et al.* suggest that the rotor tip speed of 250 m/s be the upper limit for applying PM machines in favor of solid rotor induction machines. This design value does not directly connect the tip speed to the sleeve stress. Certain design choices, particularly magnet thickness and rotor construction, can influence the sleeve stress dramatically but have no effect on tip speed. For this reason, it is the sleeve stress that determines the limit of rotor containment (and ultimate speed), and the tip speed should only be used as a parametric indicator or rule of thumb. Gilon [5] limits the useful range of wound-field synchronous machines to 8000 r/min but does not tie that to a rotor diameter or power rating.

TABLE I
REQUIRED SPECIFICATION OF HIGH-SPEED MEDIUM-VOLTAGE MOTOR

Item	Specification
Power Rating	8 MW
Rated Speed	15 kRPM
Overspeed	18 kRPM
Drive Rating	6.6 kV, 1 kA
Sleeve Configuration	Wound Carbon Fiber
Cooling Configuration	Water/Glycol Stator Jacket Curtain Air Flow over End-Turns Stator Mid-Stack Air Flow
Bearing Configuration	2-Radial, 1-Thrust Magnetic Bearing Ball Bearing for Touch Down -or- 2 Duplex Pairs of Angular Contact Oil Lubricated Ball Bearings

The assessment of Arkkio *et al.* [6] that solid rotor induction machines suffer from both poor efficiency and low power factor when compared to PM machines is corroborated by Gilon [5] who cites the low efficiency of solid rotor induction machines and Walter *et al.* [8] who present performance data for such a machine that shows, even at partial load, that the power factor is quite low (less than 0.7). However, it is not clear how much power factor reduction is due to the selection of the rotor construction and how much is due to the choice of pole count (a two-pole machine versus the four-pole machine presented herein and that of Weeber *et al.* [3]).

The high-speed sleeved PM machine has an intrinsically larger magnetic air gap than the unsleeved PM machine due to the sleeve thickness and the increased magnet thickness required to force an equivalent amount of flux through the larger magnetic gap. This larger magnetic gap provides better demagnetization protection, particularly under short-circuit conditions.

With the higher power density and frequency of high-speed machines also comes higher loss density. Special attention must be paid to the choice of lamination material, coil construction, and cooling system for what would otherwise be a typical stator and housing design. The potential of PM machines to demagnetize under extreme temperature is often used as a factor in dismissing them for applications where robustness is required [7]. The choice of samarium cobalt mitigates this risk. In the case of composite sleeve machines, the maximum sleeve operating temperature represents another design constraint which may supersede the magnet material selection. The machine design presented here benefits from a relatively large magnetic gap and near immunity to demagnetization.

II. DESIGN SPECIFICATION

The petrochemical industry would benefit from a high-speed medium-voltage PM machine to drive centrifugal compressors or be directly driven by gas turbines (Table I). The PM machine has a reduced system weight, higher operating efficiency, and smaller envelope than a conventional solution [7]. Directly coupling the motor to the compressor or the generator to the turbine eliminates the need for a gearbox and its inherent maintenance costs and performance penalties. By utilizing magnetic bearings, the machine maximizes the benefits of a lube-free system. Magnetic bearings can operate at higher speeds with less loss than certain types of mechanical bearings, which are constrained by size and lubrication type.

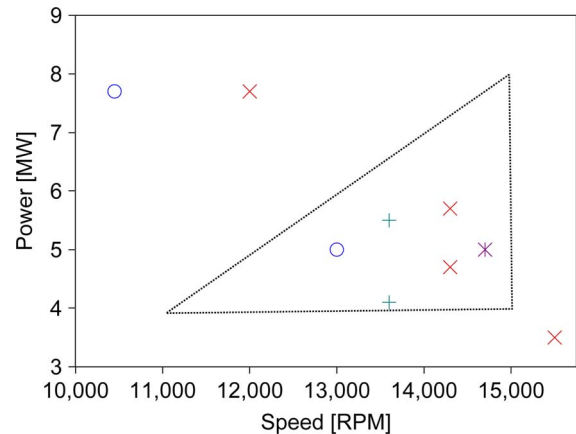


Fig. 1. Gas turbine ratings from various manufacturers [11]. The triangle shows the target applications for a product family rated at 8 MW and 15 000 r/min maximum.

Fig. 1 shows a selection of gas turbine ratings which are well matched to an 8-MW product family operating at a rated speed of no more than 15 000 r/min.

III. DESIGN AND ANALYSIS

A. Electromagnetic Sizing

The electromagnetic sizing of the machine tends to be of secondary importance, behind the mechanical limits of the rotor. The operational speed is driven by market analysis (Fig. 1), and a rotor tip speed rule of thumb is used as a starting point for the rotor design. The rotor diameter is selected ultimately by iterating between the rotor containment and electromagnetic analyses. The rotor dynamic response determines the maximum rotor length and, hence, the power limit for the product family. The stator design follows conventional lines, initially using a target current density and finally a detailed thermal analysis based on the electromagnetic loss estimate.

B. Electromagnetic Losses

Although the stator is very similar in construction to a conventional machine, a few loss mechanisms must be specifically addressed. Relatively thin low-loss silicon steel is used to contain losses under the high-frequency operation. Special care must be taken in selecting the strand configuration in the multistrand multiturn form-wound coils to contain strand losses under high-frequency operation. Commercially available lumped-parameter circuit simulators with core loss and copper eddy-loss models were used to predict stator losses. These calculations were compared to results obtained with a commercial electromagnetic finite-element-analysis (FEA) software and published closed-form analytical methods.

Rotor losses due to eddy currents were predicted using a time-stepping rotating-grid solver from the same commercial FEA software. The solution was obtained with a 2-D analysis that ignored the axial segmentation of the magnets and the electrical isolation between each other and the shaft. This approach overstates the losses, and they were found to be insignificant when compared to the rotor windage.

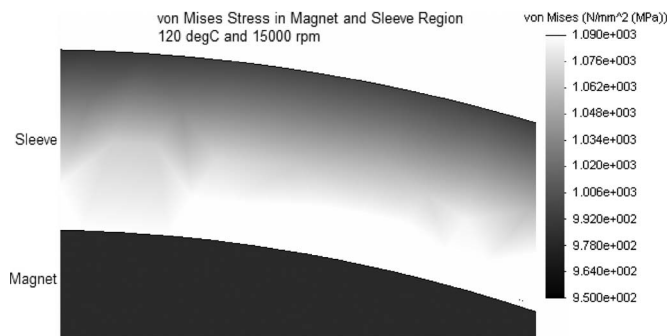


Fig. 2. Von Mises stress distribution at 15 000 r/min and 120 °C.

C. Rotor Containment

A FEA tool is used to model the rotor geometry including a rotor hub, magnets which are sized by the electromagnetic design, and an initial sleeve design. Hoop stress in the sleeve, von Mises stress in the magnets and sleeve (Fig. 2), and contact pressure between the rotor shaft and magnets and between the magnets and sleeve are analyzed at varying speeds and temperatures. Rotor geometry is modified, and the analysis iterated until the stresses and pressures fall within design limits.

The rotor geometry is then set and can be used to determine the rotor-winding process variables including tape and rotor temperature, tape tow tension, and number of tape layers.

The rotor-containment model can then be verified by rotor burst testing. Previous rotor burst-testing results coupled with tensile-strength tests conducted on wound rings of the carbon-fiber tape determined the material-stress limits and, therefore, the rotor-containment sleeve-design limits used. Additional burst-testing data are added to the data already collected and increases the statistical accuracy of the design limits.

While the rotor tip speed for this design follows the rule of thumb of 250 m/s, the maximum allowable sleeve stress is constrained by the limits of the material and is above that chosen by Arkkio [6].

D. Rotor Dynamics

A commercially available rotor-dynamics software package is used to determine the mechanical limits of the machine, such as bearing span, by predicting its dynamic behavior. The solution approach of the software is to lump the mass and inertia of a defined area to create the nodes connected by massless beams.

Two separate configurations are discussed: a rotor supported by magnetic bearings and a rotor supported by ball bearings in a resilient mount. The bearings for both configurations are modeled as dynamic supports with variable stiffness and damping.

The magnetic-bearing configuration (Fig. 3) consists of two radial-support bearings, one at either end of the shaft and a separate active-thrust bearing at the coupled end to compensate for any axial loading of the coupled system. Touchdown bearings for startup and shutdown operations are grease-lubricated ceramic-ball bearings. A coupling appropriate to the machine size was chosen and its half-weight was modeled as a cantilevered weight. Due to the nature of magnetic bearings,

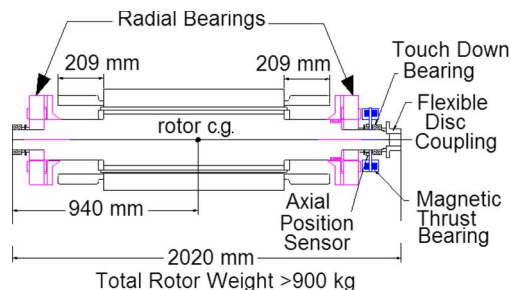


Fig. 3. Magnetic bearing and rotor layout.

the main-housing support structure does not affect the rotor-dynamic performance and therefore is not included in the system-level model.

The ball-bearing configuration consists of oil-lubricated and oil-cooled angular-contact ceramic-ball bearings that are preloaded in a back-to-back arrangement. The preloaded ball bearings are mounted in an oil squeeze-film damper for load reduction. As with the magnetic-bearing configuration, a coupling half-weight is added to the drive end of the machine as a cantilevered weight. The stiffness and damping of the resilient mount is included in the system-level model; however, the frame is considered infinitely stiff and is therefore not included.

The rotor itself is modeled with the solid rotor hub as the only source of stiffness; the magnets and sleeve are modeled as parasitic weight at the proper diameter. Based on the modal impact testing of rotors built previously, it is known that the magnets and sleeve do add some stiffness to the rotor. This stiffness is difficult to predict exactly due to variations in the magnet bonding and sleeve winding process from rotor-to-rotor and is therefore neglected, creating an inherent margin in the analysis. This is a very conservative approach and is the standard design practice.

The total rotor weight for this machine is slightly over 900 kg, and the bearing span is approximately 1.6 m. The machine with either bearing configuration is designed to run subcritical or below the first forward-bending mode. The PM machine’s solid rotor-shaft construction is what allows the machine to run at such high speeds and maintain subcritical operation. This is in contrast to a traditional wound-field synchronous-machine or a squirrel-cage induction machine that in order to maintain subcritical operation must run at lower speeds. Additional design margin can be obtained by limiting the bearing span and maintaining the rotor hub OD as large as possible in the stator end-turn region.

The magnetic-bearing configuration resulted in a first forward-bending mode of 22 391 cycles per minute (cpm) (Fig. 4).

The ball-bearing configuration resulted in a first forward-bending mode of 21 768 cpm (Fig. 5). Both configurations are viable since the first forward-bending mode falls more than 20% above the overspeed of the machine.

The magnetic-bearing control-circuit design depends heavily on the expected system load response at the location of the support-bearing actuators. The bearing load-response plots are also important to the ball-bearing configuration since this indicates the vibration that will be seen during operation.

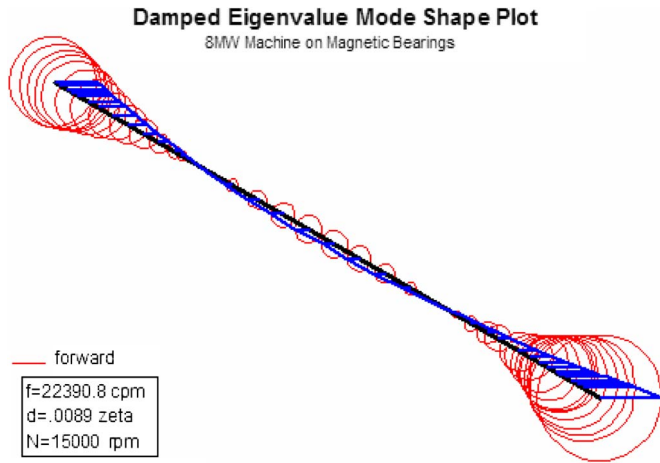


Fig. 4. Mode shape for the first forward-bending mode of magnetic-bearing configuration.

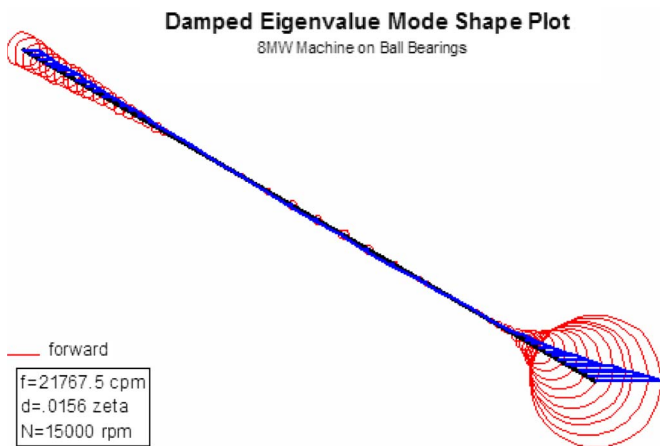


Fig. 5. Mode shape for the first forward-bending mode of ball-bearing configuration.

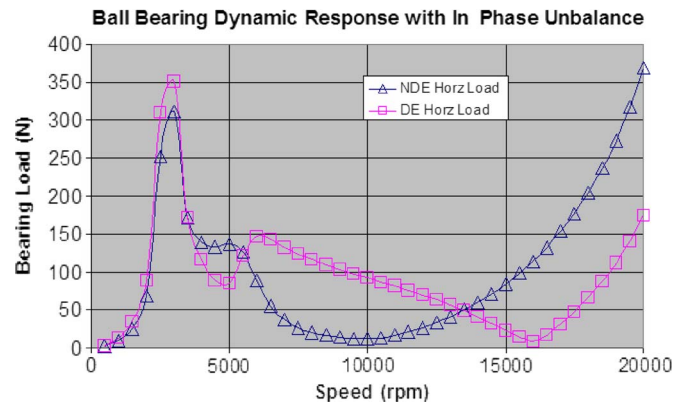


Fig. 7. Bearing load response plot for ball-bearing configuration.

E. Cooling

A lumped-parameter model is used to model the machine geometry including rotor, stator, and cooling jacket to prescreen cooling system topologies. Finally, a computational-fluid-dynamic (CFD) model of the system was used to determine the machine operating point. A maximum design temperature limit for coil insulation and carbon-fiber analysis was set at 150 °C.

A separate aluminum cooling jacket with a press fit to the stator back iron extracts heat through a water/glycol cooling flow. The interference fit is selected for structural integrity as well as to reduce the insulating effects of a microscopic air gap, or contact resistance, between the cooling jacket and the stator back iron.

Curtain-air flow removes heat out of the end turns without being choke limited by the radial air-gap size. Although the wound-carbon-fiber sleeve acts as a thermal insulator, cooling flow through the radial air gap provides some cooling to the rotor as well as to the stator tooth tips; therefore, cooling air flow is actively blown through a mid-stator-stack vent and into the radial air gap and out over the stator end turns (Fig. 8). Loss input is determined and allocated from the electromagnetic analysis tools discussed in Section IV-B.

The CFD analysis tool utilizes the actual 3-D solid-assembly model. Losses are represented as heat flux on the surface of the appropriate component; for example, windage losses are modeled as heat flux on the surface of the rotor-containment sleeve. Cooling-flow inlets and outlets are defined; however, the actual path and velocity of the flows were calculated by the CFD model (Fig. 9). The conclusions of the lumped-parameter model were confirmed and refined by the CFD analysis.

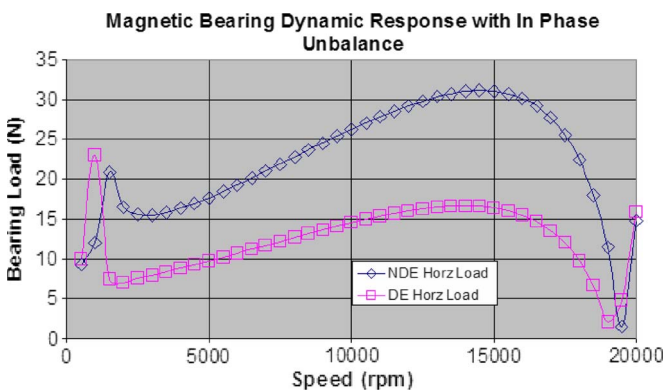


Fig. 6. Bearing load response plot for magnetic-bearing configuration.

The response plots shown, magnetic-bearing (Fig. 6) and ball-bearing (Fig. 7) configurations, are based on four times the maximum allowable imbalance per ISO 1940/1-1986 machine category G2,5 in phase with each other with a two-plane balancing scheme. There are no major gyroscopic effects for either configuration and the bearing coefficients are symmetric. Therefore the horizontal and vertical responses are identical and only the horizontal responses are shown for clarity.

IV. EXPERIMENTAL RESULTS AND MODEL VALIDATION

A. Electromagnetic Model

Nelson *et al.* [12] presented the details of the 2-MW high-speed alternator (HSA) which was used to validate the electromagnetic analysis tools prior to the prototype-machine build. The higher-than-predicted rotor-field strength reported by Nelson *et al.* was taken into account when designing the 8-MW machine by adjusting the magnet material properties, both in the drawing tolerance and in the electromagnetic model.

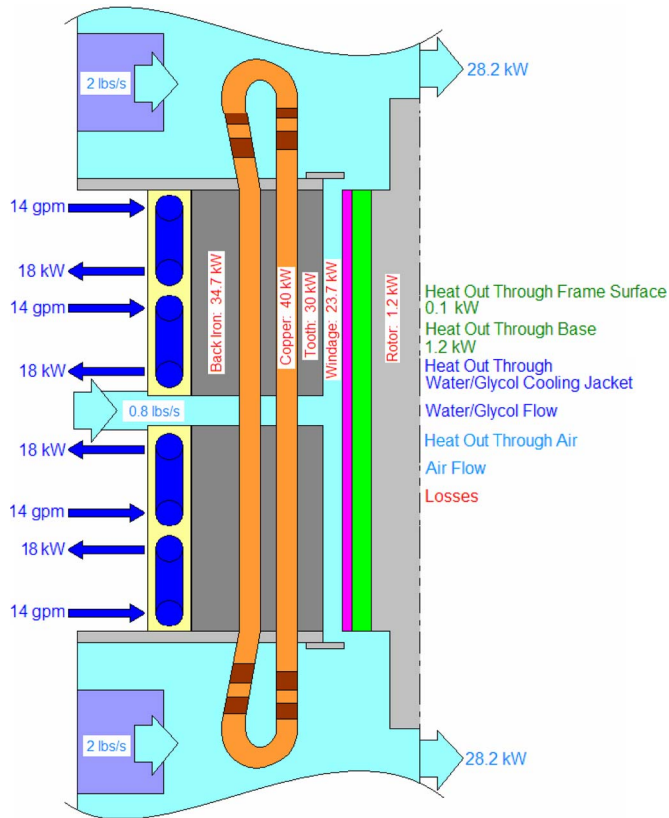


Fig. 8. Machine cross section showing cooling system.

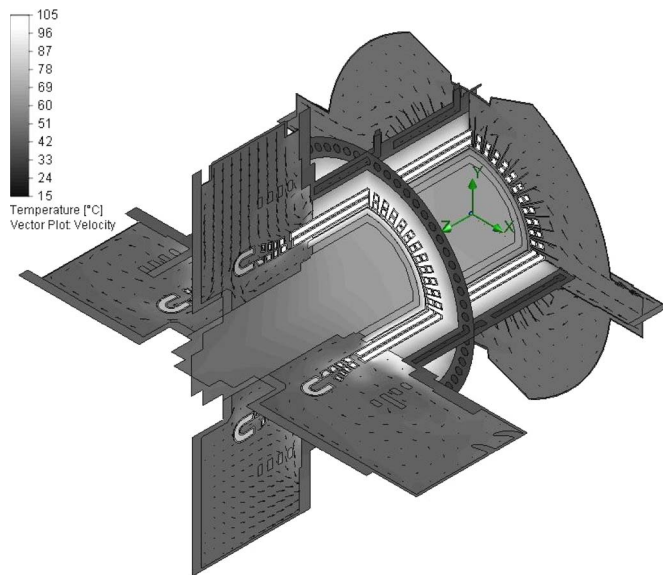


Fig. 9. Solid model results from CFD analysis of machine.

Electromagnetic aspects of the stator design are similar to or no different than a conventional machine, and therefore, the model validation of stator quantities is of lesser concern and is not presented here. Detailed experimental-design verification was carried out after the 8-MW machine was built and presented in [13] which includes open-circuit, short-circuit, no-load, and partial-load tests. It was shown that the open-circuit voltage was linear with speed both before and after a series

TABLE II
TEST CONFIGURATION FOR COOLING MODEL VALIDATION

Test Set-up	Load [kW]	Liquid Cooling	Air Cooling
1	450	Yes	Yes
2	No Load	Yes	Yes
3	No Load	Yes	No
4	No Load	No	Yes

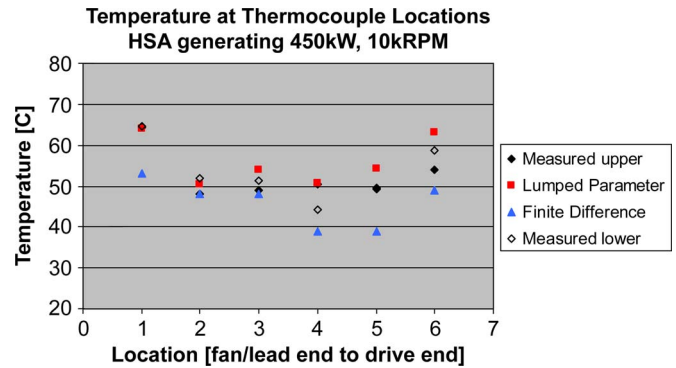


Fig. 10. Comparison plot of analytical prediction and test data.

TABLE III
LOSS SEGREGATION FOR 15 000-r/min OPERATION

	Iron Loss [kW]	Slot Cu Loss [kW]	End-turn Cu Loss [kW]	Windage [kW]	Total Loss [kW]
No-Load	29.9	16.8	0.0	16.3	63.0
3MW Generating	33.6	21.2	1.8	17.8	74.4

of sudden-short-circuit tests and that no demagnetization was detected, as expected from the HSA results.

B. Thermal Model

The machines discussed by Nelson *et al.* [12] were used as part of the thermal-model verification. Two HSA machines were coupled together in a back-to-back configuration with one operating as a motor driving and the other driven as a generator for testing purposes. In this configuration, the cooling system was adjustable and thoroughly instrumented. The HSA machines were run with different cooling and load combinations per Table II. Both the lumped-parameter and CFD models were refined based on these tests until they reasonably matched the test data (Fig. 10). In this way, the lumped-parameter and CFD models were verified. The lessons learned from the HSA testing and modeling such as the significance of the heat lost to the ambient air and through the machine feet were incorporated into the 8-MW cooling system design.

More detailed CFD models were built and compared to the actual test data of the 8-MW machine. As presented in [13], the thermal model was employed extensively to refine the loss allocation over the operating range. The heat balance showed higher losses than initially predicted, and correlation with temperature measurements allowed the final segregation of those losses and, later, correction of the analytical methods used to determine those losses. The loss segregation by CFD is presented in Table III.

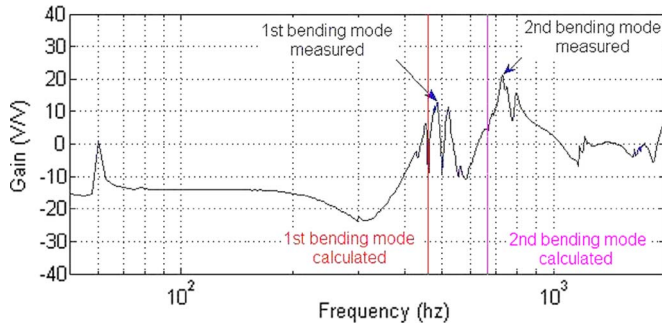


Fig. 11. Rotor impact modal test results.

C. Rotor Dynamic Model

The rotor was hung vertically and subjected to a modal-impact test to validate the rotor-dynamic model. Since the rotor is modeled such that the magnets and carbon-fiber sleeve add no stiffness to the overall model, the predicted natural frequencies should be lower than the measured natural frequencies which were confirmed (Fig. 11). Overall, the rotor and bearing support system for the ball-bearing configuration behaved close to predicted levels, confirming that the analysis method was appropriate for the design. Further details are available in [13].

V. CONCLUSION

This paper has presented a viable medium-voltage high-speed PM machine design well suited for the replacement of, or coupling with, a variety of gas turbines.

The machine's stator consists of thin low-loss silicon-steel laminations and multistrand multiterm form-wound coils and was designed for high-frequency operations using a commercially available FEA program.

The machine will be supported by either one thrust and two radial magnetic bearings with ball bearings used as touchdown bearings during startup and shutdown or two duplex pairs of oil-lubricated angular-contact bearings. The rotor-dynamic analysis completed shows the machine to be running subcritical with a first forward-bending mode that is 20% above the overspeed condition and over 20% above the nominal operating speed for both configurations. The response plots show acceptable bearing loads based on the bearing support structures for each configuration.

Cooling for the machine consists of cooling air entering through a midstator vent as well as independent cooling flows over each of the end-turn sections and a water/glycol cooling flow through a pressed-on cooling jacket on the stator outer diameter. By independently blowing cooling air over the end turns, the total flowrate is not restricted to the rotor air-gap choke flow and can be significantly increased to meet the thermal requirements of the machine.

The analytical tools used in the design have been validated with hardware. Future design improvements should be focused on trading the cost and complexity of improved cooling system designs against using more costly lower loss materials such as stator laminations, conductors, and higher energy product magnets, or even a gross machine size increase to reduce the loss density.

REFERENCES

- [1] B. M. Wood, C. L. Olsen, G. D. Hartzo, J. C. Rama, and F. R. Szenasi, "Development of an 11000-r/min 3500-hp induction motor and adjustable-speed drive for refinery service," *IEEE Trans. Ind. Appl.*, vol. 33, no. 3, pp. 815–825, May/Jun. 1997.
- [2] S. C. LaGrone, M. C. Griggs, and M. Bressani, "Application of a 5500 rpm high speed induction motor and drive in a 7000 hp natural gas compressor installation," in *Proc. 39th Annu. Petroleum Chem. Ind. Conf.*, Sep. 28–30, 1992, pp. 141–146.
- [3] K. Weeber, C. Stephens, J. Vandam, J. Yagielski, A. Gravame, and D. Messervey, "High-speed permanent-magnet motors for the oil & gas industry," in *GT-28282; ASME Turbo Expo: Power Land, Sea Air*, May 14–17, 2007, pp. 1–10.
- [4] N. Shade, "New compression and power applications," *Compressor Tech Two*, pp. 20–26, Mar. 2008.
- [5] D. C. Gilon, "Design and tests of a 6-MW, 10000 rpm induction motor," in *Proc. 5th Int. Conf. Elect. Mach. Drives*, Sep. 11–13, 1991, pp. 6–10.
- [6] A. Arkio, T. Jokinen, and E. Lantto, "Induction and permanent-magnet synchronous machines for high-speed applications," in *Proc. 8th ICEMS*, Sep. 27–29, 2005, vol. 2, pp. 871–876.
- [7] S. Evon and R. Schiferl, "Direct drive induction motors," in *Conf. Rec. Annu. Pulp Paper Ind. Tech. Conf.*, Jun. 27–Jul. 1 2004, pp. 49–54.
- [8] H. Walter, A. Moehle, and M. Bade, "Asynchronous solid rotors as high-speed drives in the megawatt range," in *Proc. IEEE PCIC*, Sep. 17–19, 2007, pp. 1–8.
- [9] M. J. Melfi, S. D. Rogers, S. Evon, and B. Martin, "Permanent magnet motors for energy savings in industrial applications," in *Proc. 53rd Annu. Petroleum Chem. Ind. Conf.*, Sep. 11–Oct. 15 2006, pp. 1–8.
- [10] N. Bianchi, S. Bolognani, and F. Luise, "Potentials and limits of high-speed PM motors," *IEEE Trans. Ind. Appl.*, vol. 40, no. 6, pp. 1570–1578, Nov./Dec. 2004.
- [11] "2004 basic specifications—Mechanical drive gas turbine engines," *Compressor Tech Two*, pp. 115–117, 2004.
- [12] A. Nelson, M. Baker, C. Huynh, L. Hawkins, and A. Filatov, "New developments in high-speed, direct-connected, permanent magnet motors and generators for marine applications," in *Conf. Rec. WMTC*, Mar. 6–10, 2006.
- [13] D. M. Saban, C. Bailey, D. Gonzalez-Lopez, and L. Luca, "Experimental evaluation of a high-speed permanent-magnet machine," in *Proc. 55th IEEE PCIC*, Sep. 22–24, 2008, pp. 1–9.



Cassandra Bailey (M'08) received the B.S. degree in mechanical engineering from Northwestern University, Evanston, IL, in 2003.

She was an Integrated Drive Generator Design Engineer with Hamilton Sundstrand, designing an integrated variable-speed transmission and ac generator for various military aircraft applications. Currently, she is with Direct Drive Systems, Cerritos, CA, as a Project Engineer, designing high-speed medium-voltage permanent-magnet machines.

Ms. Bailey is a member of the American Society of Mechanical Engineers.



Daniel M. Saban (S'90–M'93–SM'06) received the B.S.E.E. degree from the University of Illinois, Urbana–Champaign, in 1992, the M.S.E.E. degree from Purdue University, West Lafayette, IN, in 1993, and the M.S.E.E. and M.S.M.E. degrees with focuses on power electronics and controls, respectively, and the Ph.D. degree in electrical engineering, with specialization in electric motor analysis, from the University of Wisconsin, Madison, in 2002, 2003, and 2006, respectively.

He is currently the Director of Technology with Direct Drive Systems, Cerritos, CA. He was previously with Hamilton Sundstrand and General Electric (concurrent with his advanced degrees). Throughout his 16-year career, he has been involved in the advanced electromagnetic design of electric machinery including new lamination and winding designs, design tools, and both prototype and product family development for commercial, industrial, and aerospace applications.

Dr. Saban is a Registered Professional Engineer in the States of Indiana and Illinois.



Paulo Guedes-Pinto (M'06) received the B.S.E.E. degree in electric machines from the University of Sao Paulo, Sao Paulo, Brazil, in 1979. He also pursued postgraduate studies in power systems and quality engineering.

He has over 17 years experience in the design and manufacture of motors and generators with Industrias Villares, Brazil. He is currently with Direct Drive Systems, Cerritos, CA.

Mr. Guedes-Pinto is a Registered Professional Engineer in the Province of Ontario, Canada.